

Article

Sorption of Pb(II) from Aqueous Solutions by Acid-Modified Clinoptilolite-Rich Tuffs with Different Si/Al Ratios

Mohamed Abatal ¹, Atl V. Córdova Quiroz ², María T. Olguín ^{3,*},
América R. Vázquez-Olmos ⁴, Joel Vargas ⁵, Francisco Anguebes-Franseschi ²
and German Giacomán-Vallejos ⁶

¹ Facultad de Ingeniería, Universidad Autónoma del Carmen, C.P. 24180 Ciudad del Carmen, Campeche, Mexico; mabatal@pampano.unacar.mx

² Facultad de Química, Universidad Autónoma del Carmen, Calle 56 No. 4 Esq. Av. Concordia, Col. Benito Juárez, C.P. 24180 Ciudad del Carmen, Campeche, Mexico; aquiroz@delfin.unacar.mx (A.V.C.-Q.); fanguebes@pampano.unacar.mx (F.A.-F)

³ Departamento de Química, Instituto Nacional de Investigaciones Nucleares, Carretera México-Toluca s/n. La Marqueza, Ocoyoacac, C.P. 52750 Estado de México, Mexico

⁴ Instituto de Ciencias Aplicadas y Tecnología, UNAM, Circuito Exterior, S/N, Ciudad Universitaria, A.P. 70-186, Delegación Coyoacán, C.P. 04510 Ciudad de México, Mexico; america.vazquez@ccadet.unam.mx

⁵ Instituto de Investigaciones en Materiales, Unidad Morelia, Universidad Nacional Autónoma de México, Antigua Carretera a Pátzcuaro No. 8701, Col. Ex Hacienda de San José de la Huerta, C.P. 58190 Morelia, Michoacán, Mexico; jvargas@iim.unam.mx

⁶ Facultad de Ingeniería, Universidad Autónoma de Yucatán, Av. Industrias no Contaminantes por Periférico Norte, Cordemex, C.P. 97310 Mérida, YUC, Mexico; giacomán@correo.uady.mx

* Correspondence: teresa.olguin@inin.gob.mx; Tel.: +52-555-329-7200 (ext. 12265)

Received: 15 April 2019; Accepted: 9 June 2019; Published: 13 June 2019



Abstract: The removal of Pb(II) from aqueous solutions by acid-modified clinoptilolite-rich tuff was investigated in this work. Clinoptilolite-rich tuff samples were treated using H₂SO₄ at different concentrations. Prior to and following acid treatment, the samples were characterized using X-ray diffraction (XRD), scanning electron microscopy (SEM), energy dispersive X-ray spectroscopy (EDS), and Fourier-transform infrared spectroscopy (FTIR). The pH of the point of zero charge (pH_{PZC}) was also determined as part of this characterization. Batch studies were studied to investigate Pb(II) removal as a function of contact time, initial Pb(II) concentration, adsorbent dosage, and solution pH. The results of the XRD and SEM techniques showed that clinoptilolite is the main mineral of the non- and acid-treated natural zeolite samples. However, EDS analysis indicated that the Si/Al ratio increases as the exchangeable ions decrease with increasing acid concentrations. The optimum conditions for Pb(II) removal for samples with $4.37 \leq \text{Si/Al} \leq 7.9$ were found to be as follows: Contact time of 60–360 min, pH: 6–8, and adsorbent dose of 6 mg g⁻¹; whereas for acid-modified clinoptilolite-rich tuffs with $9.01 \leq \text{Si/Al} \leq 9.52$, these conditions were as follows: Contact time of 1440 min, pH: 8–10, and adsorbent dose of 10 mg g⁻¹. The experimental data were analyzed by kinetic and isotherms models. The results showed that the sorption of Pb(II) on samples with Si/Al ratios of 4.37, 5.31, and 7.91 were in agreement with the pseudo-second order and Langmuir isotherm with $q_m = 48.54, 37.04, \text{ and } 14.99 \text{ mg g}^{-1}$, respectively, while the kinetic data and isotherm for samples with $9.01 \leq \text{Si/Al} \leq 9.52$ were found to fit the pseudo-first order and Freundlich model.

Keywords: lead; sorption; natural zeolite; clinoptilolite; sulfuric acid

1. Introduction

Zeolites are hydrous and crystalline aluminosilicate minerals with a regular and microporous structure (pore size from 3.0 to 10 Å) [1]. Their frameworks are comprised of tetrahedral building units TO_4 ($T = \text{Si or Al}$), connected together by sharing one oxygen atom at the corners to form complex three-dimensional open networks of channels or cavities and cages (0.2–1.2 nm) occupied by H_2O molecules and exchangeable cations [2]. The partial substitution of Si^{4+} by Al^{3+} in the zeolite framework produces a negative charge that is often neutralized by the exchangeable alkali and/or alkaline earth cations (Na^+ , K^+ , Ca^{2+} , Sr^{2+} , or Ba^{2+}) [3] or by H^+ [4] for acidic zeolite in order to maintain electrical neutrality throughout the structure. Natural zeolites exhibit interesting structural properties such as a large specific surface, flexibility, and well-defined micropores in molecular dimensions, as well as high chemical and physical stability (e.g., thermal and mechanical) [5], and sorption characteristics obtained by combined ion-exchange and molecular-sieve properties [6]. These outstanding properties allow these materials to offer promising applications in many sustainable processes such as wastewater treatment [7] and petroleum refining [8] as well in agriculture and construction [9]. Over the last decades, many researches have focused on clinoptilolite due to its attractive selectivity for toxic metal cations and organic substances [6,10–14]. It was reported that the ion-exchange process in natural zeolites depends on factors related to adsorbate and adsorbent characteristics such as pH and temperature of the solution, ion concentration, crystal structure, and chemical composition of the zeolitic material [10,15]. The cation exchange capacity (CEC) of a zeolite is directly dependent on the Si/Al ratio [16]. This important property of the natural zeolites can be used to remove heavy metals from polluted water. For instance, the lead (Pb^{2+}) is a toxic metallic species which is necessary to eliminate from the environment [17].

It was also reported that a variation in the SiO_2/Al_2O_3 ratio of the natural zeolites affects the hydrophilicity/hydrophobicity of this material, which is correlated with the adsorption, catalysis, and ion exchange properties [18,19]. Zeolite dealumination using acid as a chemical agent allows zeolites with a higher SiO_2/Al_2O_3 ratio to be obtained, which are usually used for the removal of organic hydrophobic contaminants in water [20] and volatile organic compounds in air [21]; whereas alkali treated zeolite using organic hydroxides [22] or sodium hydrate [16,23] can achieve materials with a lower SiO_2/Al_2O_3 ratio for the removal of ammonium [24] and heavy metals [6,25].

In previous studies [16,18,19,22,23,25–30], the researches focused mainly on the effect of the SiO_2/Al_2O_3 ratio on the structural properties of zeolites. Moreover, these studies used synthesized zeolites [19,22,26–28,30], whereas the only raw zeolites used being mordenite and clinoptilolite. Kussainova et al. [31] reported the Pb(II) removal from an acid media. However, there was no information in the literature about the adsorption behavior of this heavy metal using acid modified natural zeolites. Therefore, the main objective of this research was to know the correlation between the Si/Al ratio and the Pb(II) removal capacity from aqueous solutions using non- and acid-modified clinoptilolite-rich tuffs. In addition, the structural and morphological properties of the materials were studied by XRD, SEM, and IR techniques. This study was aimed to evaluate the influence of contact time, initial pH, adsorbent dosage, and initial concentration on the removal of Pb(II) from aqueous solutions.

2. Materials and Methods

2.1. Clinoptilolite-Rich Tuff and Conditioning

A clinoptilolite-rich tuff from Villa de los Reyes (San Luis Potosí State, Mexico) was sieved for a particle size of 40 mesh and washed at 25 °C several times with deionized water ($18.2 \text{ M}\Omega \text{ cm}^{-1}$, resistivity) to remove any water-soluble impurities. After vacuum filtration, the clinoptilolite-rich tuff was dried at 80 °C overnight. This sample was named Nat-CLI. Acid treatment was carried out by treating the Nat-CLI with 0.1 M, 0.2 M, 0.5 M, and 1 M H_2SO_4 (95–98%, J. T. Baker) with a liquid/solid ratio of 1:20. The suspensions were stirred at 90 °C for 4 h and then the solids were vacuum filtered and

washed with excess deionized water until the pH of the rinse water was reduced to 6 approximately. Finally, the samples were dried at 80 °C for 12 h and denoted as HCLI-0.1M, HCLI-0.2 M, HCLI-0.5 M, and HCLI-1.0 M, respectively.

Deionized water was used to prepare synthetic stock solutions (500 mg L⁻¹) of Pb(II) using PbCl₂ (98%, Sigma-Aldrich Co, St. Louis, MO, USA). The desired concentrations were prepared from the dilution of the stock solution using deionized water. The pH of each was adjusted with 0.1 M HCl or 0.1 M NaOH.

2.2. Samples Characterization

X-ray diffraction (XRD) analysis was carried out using an APD 2000 PRO X-Ray diffractometer with CuK_α radiation. The patterns of the samples were recorded between 6° and 60° 2θ with a scanning speed of 0.025 degrees s⁻¹ and step time of 10 s. Scanning electron micrographs were obtained with a HITACHI S-3400N scanning electron microscope (SEM) and the chemical composition was determined by energy-dispersive X-ray spectroscopy at different points on the surface of the samples. The working conditions of the SEM-EDS were 10 kV for the energy dispersive analysis, with a current intensity of 30 pA, and work distance of 10.6 mm. Fourier transformed infrared (FTIR) spectroscopy was conducted using a Nicolet Nexus 670 FT-IR infrared spectrometer from 4000 to 400 cm⁻¹ with a resolution of 4 cm⁻¹ in a KBr (spectroGrade, Merk KGaA, Darmstadt, Germany) wafer.

The pHPZC was obtained using batch equilibration technique [12]. The samples were introduced into Erlenmeyer flasks containing 0.01 M NaCl solution with a solid/solution ratio of 1:500. The initial pH was adjusted from 2 to 12 by adding a few drops of 0.5 M HCl or 0.1 M NaOH. The mixtures were shaken for 24 h at 24 °C and the final pH values of the filtered suspensions were measured using Thermo Scientific pH-meter (ORNION 3star pH Benchtop). Plots of pH_{initial} vs. pH_{final} were constructed and the pHPZC was determined from the intersection of these curves.

2.3. Sorption Experiments

2.3.1. Kinetic

The kinetic behavior was determined using a batch technique. 10 mL of Pb(II) aqueous solution with a known initial concentration (100 mg L⁻¹) were added to 0.10 g of non- and acid-modified clinoptilolite-rich tuffs in a 12 mL conical flask. The mixtures were agitated at 150 rpm in an orbital shaker at 25 °C for different time intervals (15–1440 min). At the end of the each contact time, the tubes were centrifuged at 4500 rpm for 2 min, and the adsorbent was removed by filtration. The concentration of remaining Pb(II) in the supernatants was analyzed using atomic absorption spectroscopy (Thermo Scientific iCE 3000 Series).

The sorbed amount of Pb(II) (q , mg g⁻¹) was calculated by a mass balance relationship equation as follows:

$$q = \frac{(C_0 - C_t)V}{W} \quad (1)$$

where V is the solution volume (mL), W is the amount of sorbent (g), C_0 and C_t are the initial and final metal concentrations (mg L⁻¹), at time t (min).

In order to describe the kinetics of the adsorption process of Pb(II) by the zeolite materials, pseudo-first-order and pseudo-second-order models [32] were applied in this work. Lineal forms for these models are represented in Equations (2) and (3), respectively.

$$\ln(q_e - q_t) = \ln q_e - k_1 t \quad (2)$$

$$\frac{t}{q_t} = \frac{1}{k_2 q_e^2} + \frac{t}{q_e} \quad (3)$$

where q_t (mg g^{-1}) and q_e (mg g^{-1}) are the amounts of metal ions adsorbed at time t and equilibrium, respectively. k_1 (min^{-1}) and k_2 ($\text{g mg}^{-1}\text{min}^{-1}$) are the pseudo-first order and pseudo-second order reaction rate constants, respectively.

2.3.2. Isotherm

The sorption isotherm experiments were carried out in 12 mL flasks at 25 °C by placing 0.10 g of non- and acid-modified clinoptilolite-rich tuffs with 10 mL of Pb(II) aqueous solution at different initial concentrations ranging from 10 to 500 mg L^{-1} . The mixtures were agitated in an orbital shaker at 150 rpm for 24 h and after this time, the samples were centrifuged at 4500 rpm for 2 min and the metal concentrations of the supernatants were analyzed by atomic absorption spectrometry (AAS).

In this work, Langmuir and Freundlich models were applied to describe the equilibrium metal adsorption. The lineal forms for these models are expressed by Equations (4) and (5), respectively [33].

$$\frac{C_e}{q_e} = \frac{1}{q_m K_L} + \frac{C_e}{q_m} \quad (4)$$

$$\ln q_e = \ln K_F + \frac{1}{n} \ln C_e \quad (5)$$

where q_m (mg g^{-1}) is the monolayer adsorption capacity of the adsorbent, q_e is the amount of solute adsorbed at equilibrium (mg g^{-1}), C_e (mg L^{-1}) is the equilibrium solute concentration, K_L (L mg^{-1}) is the adsorption constant related to the energy of sorption. K_F (mg g^{-1})(L mg^{-1}) $^{1/n}$ and $1/n$ are empirical constants of the Freundlich isotherm.

In order to compare the results obtained for the Pb(II) sorption by the different acid-modified zeolitic materials considering each initial concentration from the isotherm, the partition coefficients (PC) were calculated as follows:

$$\text{PC} = q_e (\text{mg g}^{-1}) / C_e (\mu\text{M}) \quad (6)$$

2.3.3. Influence of Adsorbent Dosage and Effect of pH

The influence of adsorbent dosage on Pb(II) sorption was investigated by varying the concentration of the zeolitic materials from 1.0 to 10 mg L^{-1} , while keeping the initial concentration of the Pb(II) solution (500 mg L^{-1}) and agitation time (24 h) constant. The Pb(II) concentration in the remaining solution was analyzed as explained above.

The effect of pH on Pb(II) sorption by non- and acid-modified clinoptilolite-rich tuffs was studied in a pH range of 2–10. pH was adjusted with the dropwise addition of 0.1 M HCl or 0.01 M NaOH. Sorption experiments were conducted using 100 mg L^{-1} of Pb(II) with 0.10 g of sorbent and a contact time of 24 h.

3. Results and Discussion

3.1. Characterization

Figure 1 shows the X-ray diffraction (XRD) patterns of non- and acid-modified clinoptilolite-rich tuffs. It can be observed that all samples contained clinoptilolite as the principal mineral which is defined by its main characteristic peaks at $2\theta = 9.85^\circ$, 11.19° , 22.21° , 22.34° , 25.96° , and 28.09° according to JCPDS card 25-1349 [34]. Furthermore, comparative analysis of the XRD patterns did not show significant changes in the positions of most of the reflexions before and after the acid treatments. However, a decrease can be observed in the relative intensity of the reflexions of HCLI with the increase in sulfuric acid concentration from 0.1 to 1 M. These results suggest that the treatment of natural zeolite with H_2SO_4 caused some structural changes and loss of crystallinity in the clinoptilolite phase. This can be attributed to dealumination of the clinoptilolite as verified by the EDS analyses [29,35]. Wang et al. [36] present the reaction mechanism which take place when the clinoptilolite-rich tuffs are

in contact with a strong acid media (HNO_3). Basically they mention the break of the primary structure of the zeolite network and the formation of $\text{Al}(\text{NO}_3)_3$ because the dealumination of the zeolitic material. In the present work could be a similar mechanism with the formation of $\text{Al}_2(\text{SO}_4)_3$.

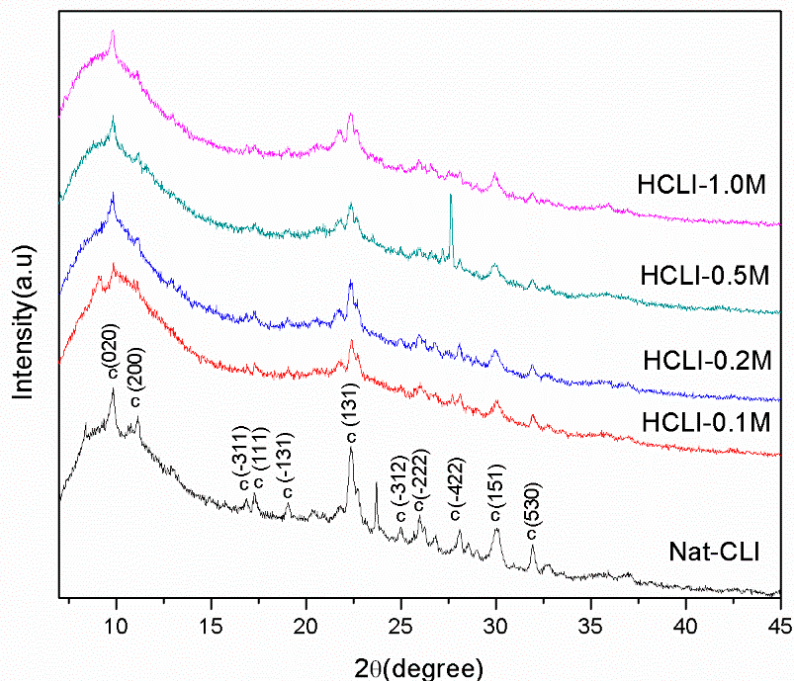


Figure 1. X-ray diffraction (XRD) patterns of non- and acid-modified clinoptilolite-rich tuffs.

The scanning electron microscopy (SEM) images of non- and acid-modified clinoptilolite-rich tuffs are shown in Figure 2. It can be observed that all of the samples presented similar morphologies and also showed the tabular and coffin shapes typical of heulandite/c clinoptilolite crystals [13]. In other investigations, the morphology of synthetic zeolite as chitosan had changed [37], whereas it remained unchanged for mordenite after chemical treatment [38]. This indicates that the change in morphology of the natural zeolites with acid treatment depends on the nature as well as the crystalline structure of these zeolitic materials.

Table 1 shows the average chemical composition expressed in terms of % weight as obtained by EDS at different points on the surface of non- and acid-modified clinoptilolite-rich tuffs. As expected, the chemical composition changed drastically following the acid treatment of natural zeolite. A total elimination of Na^+ and Mg^{2+} can be observed from the extra-framework of natural zeolite when the concentrations of H_2SO_4 are 0.1M and 0.2M, respectively; whereas the amount of Ca^{2+} and K^+ ions decrease with increasing sulfuric acid concentration as result of H^+ exchange or by the loss of Al^{3+} from the zeolite network showing that its cation exchange capacity was lost. It is clear that the H^+ is preferentially exchanged by Na^+ and Mg^{2+} from the zeolitic network rather than Ca^{2+} and K^+ and this depends of the exchangeable sites that they occupy into the zeolite network [39]. It is important to mention that the Fe could be as an associated mineral (Fe_2O_3) of the zeolitic rock.

Moreover, a significant increase in the Si/Al ratio with increasing acid concentration can be observed, due to the Al leaching from the clinoptilolite framework and the consequent loss of its crystallinity. This result is consistent with those observed by XRD analysis.

Figure 3 shows the IR spectra of the non- and acid-modified clinoptilolite-rich tuffs. The spectra have been shifted by 5% from each other starting from that corresponding to Nat-CLI in order to better appreciate the differences in the absorption bands of all the materials. A broad band appears at 3446 cm^{-1} for Nat-CLI, corresponding to the symmetric and asymmetric stretching vibration of the O-H groups, while the bending of the H-O-H vibration occurs at 1636 cm^{-1} . The strong and broad

band at 1051 cm^{-1} was assigned to the asymmetric stretching of Si-O; (from SiO_4). The weak bands of the symmetric stretching vibration observed for the O-Si-O bonds occur at 792 cm^{-1} . A weak signal can be observed at 608 cm^{-1} corresponding to bending vibrations between tetrahedrons, particularly to double ring vibrations. Finally, the band at 457 cm^{-1} corresponds to bending vibration T-O, T=Al, Si, and is related to the pore opening. These results agree well with those reported by other authors [40]. A broadening of the O-H band at 3446 cm^{-1} occurred as the acid concentration increased (from 0.1 M to 1.0 M), The bands corresponding to the Si-O and O-Si-O vibrations at 1079 cm^{-1} and 790 cm^{-1} , respectively, are more intensive. The data obtained confirm that the dealumination of clinoptilolite takes place after the acid treatment through the band near 600 cm^{-1} which was modified when the clinoptilolite was treated with the H_2SO_4 solutions indicating the break of the bond Al-O- from the zeolite network [41].

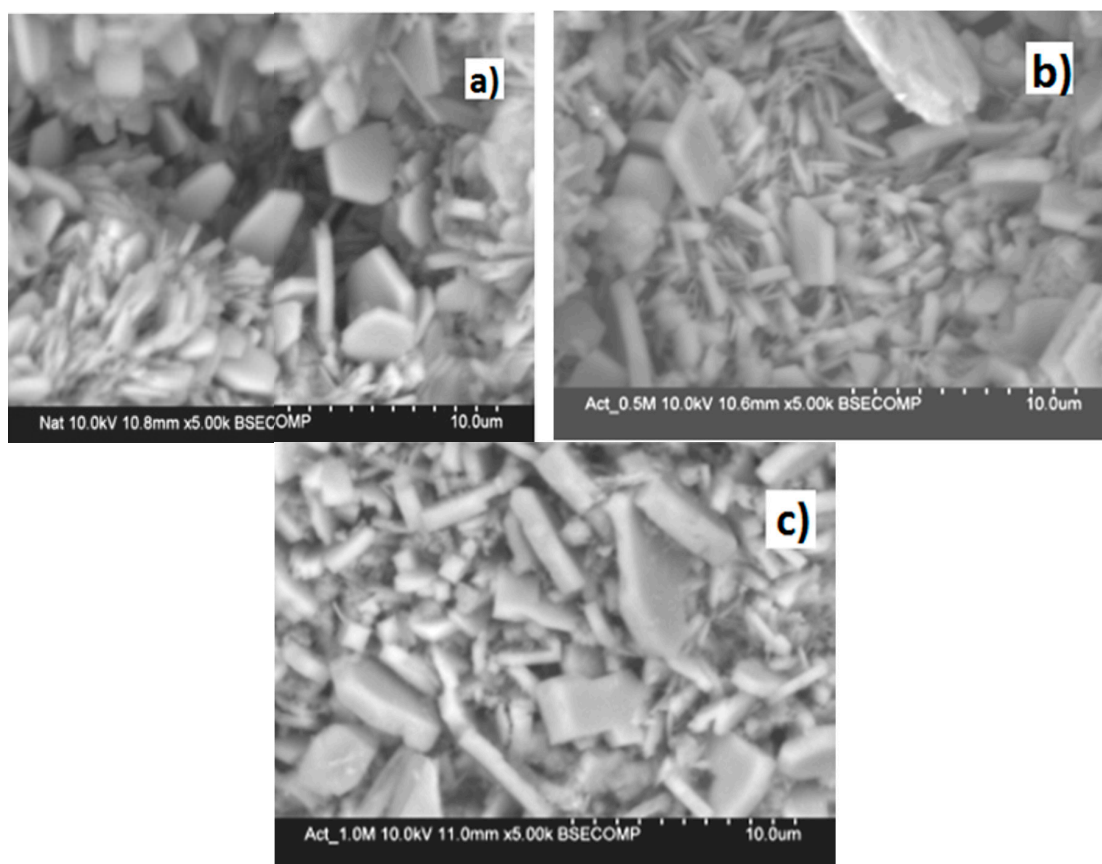


Figure 2. Scanning electron microscopy (SEM) images of (a) Nat-CLI; (b) HCLI-0.5 and (c) HCLI-1.0 M samples.

Table 1. Chemical composition (% weight) of non- and acid-modified clinoptilolite-rich tuffs.

Sample	Si/Al	Weight, %							
		O	Na	K	Ca	Mg	Si	Al	Fe
Nat-CLI	4.37	64.37	0.56	1.17	1.65	0.21	25.77	5.90	0.37
HCLI-0.1 M	5.31	66.67	0.00	0.95	0.92	0.17	26.08	4.91	0.29
HCLI-0.2 M	7.91	66.6	0.00	0.59	0.29	0.00	28.70	3.63	0.19
HCLI-0.5 M	9.04	64.06	0.00	0.49	0.52	0.00	31.37	3.47	0.09
HCLI-1.0 M	9.52	68.99	0.00	0.46	0.22	0.00	27.32	2.87	0.07

Note: Na^+ , K^+ , Ca^{2+} and Mg^{2+} are considered the exchangeable ions from the zeolite (clinoptilolite) network.

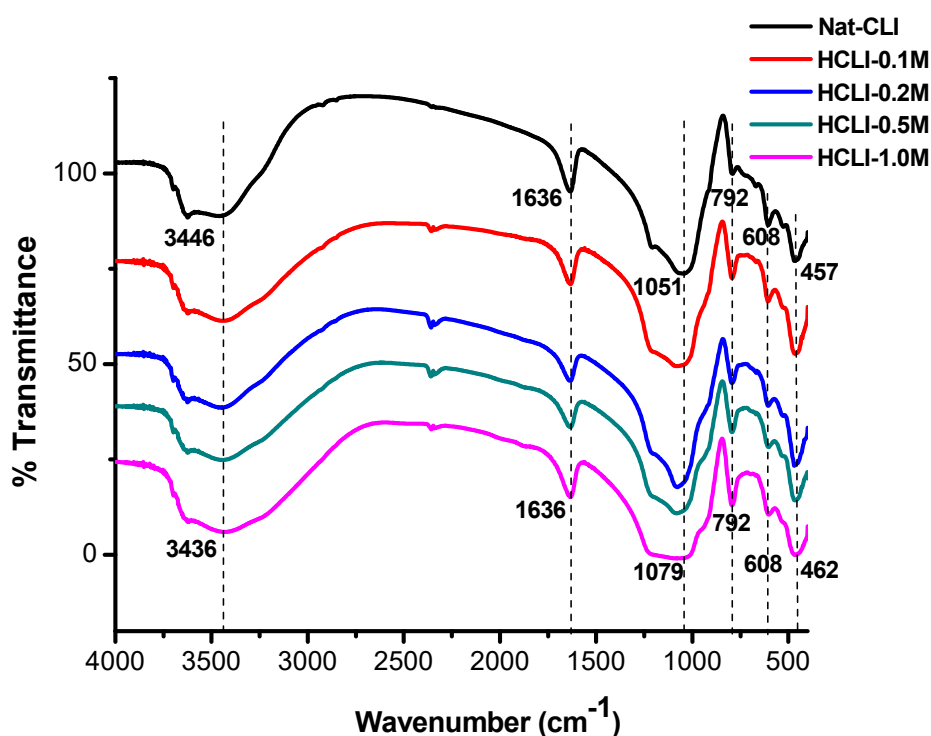


Figure 3. Fourier-transform infrared spectroscopy (FTIR) spectra of non- and acid-modified clinoptilolite-rich tuffs.

As the concentration of the acid increases (0.1 M to 1.0 M) the band due to vibration of the O-H groups, is widened and is shifted at 3436 cm^{-1} . Additionally, the band at 1051 cm^{-1} is the most affected, this also appears widened and shifted to 1079 cm^{-1} , this behavior has been attributed to a decrease in the relative content of Si/Al ratio in zeolite framework with the increase in the length of the bonds Si-O-Si(Al), and with the formation of structured effects. The other band affected is the corresponding to bending vibration T-O, T=Al, Si, this is shifted to 462 cm^{-1} , which indicates a decrease of pore opening. The observed behavior suggests that the dealumination of Nat-CLI take place after its acid treatment.

3.2. Point of Zero Charge pH (pH_{PZC})

As shown in Figure 4, the pH_{PZC} values before and after the acid-modified clinoptilolite-rich tuffs were 6.00 ± 0.01 , and 3.00 ± 0.01 , respectively. The decrease in pH_{PZC} is the result of the chemical modification of Nat-CLI by the acid treatment. Therefore, the acid-modified clinoptilolite-rich tuffs present a large pH range where the surface charge of the materials is negative (3–12), as compared to Nat-CLI (6–12). On the other hand, the chemical treatment promoted a decrease in the negative charge, and consequently, a decrease in the number of cations and the generation of very strong Lewis acid sites on the surface of the H-CLI samples. In this sense, Rožić et al. [39] reported that the following reaction took place $>Al-OH + H^+ \rightarrow >AlOH_2^+$ after the contact of the clinoptilolite-rich tuff with strong acid solutions.

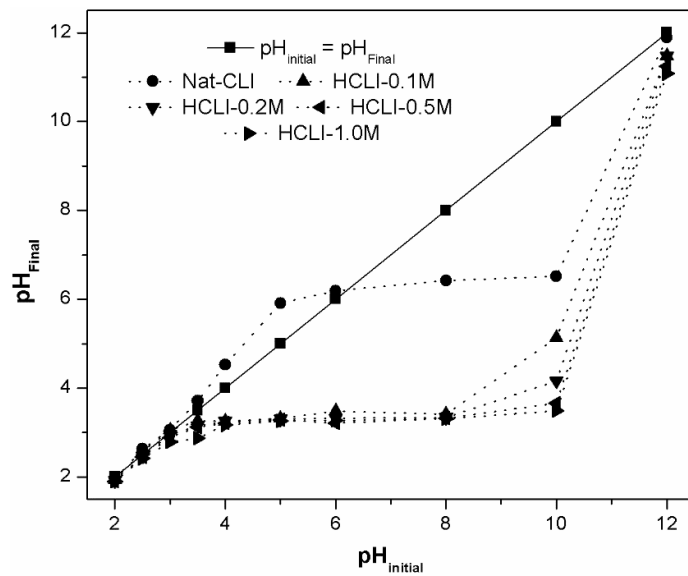


Figure 4. $pH_{initial}$ vs. pH_{final} of non- and acid-modified clinoptilolite-rich tuffs.

3.3. Kinetic

Figure 5a presents the effect of contact time on the amount of Pb(II) sorbed by non- and acid-modified clinoptilolite-rich tuffs. It can be observed that the time to reach the adsorption equilibrium increases with increasing Si/Al ratios. This can be explained by the presence of a low number of vacant active binding sites as a consequence of the Si/Al ratio increment which limited the exchange of Pb(II) by the exchangeable ions from the zeolite network. Moreover, Figure 5a shows that the kinetic processes for the Nat-CLI, HCLI-0.1 M and HCLI-0.2 M sorbents consist of two main reaction stages: An initial fast adsorption process followed by a slow continuous sorption reaction; whereas a continuous uptake of Pb(II) from aqueous solution is observed over time for HCLI-0.5 M and HCLI-1.0 M.

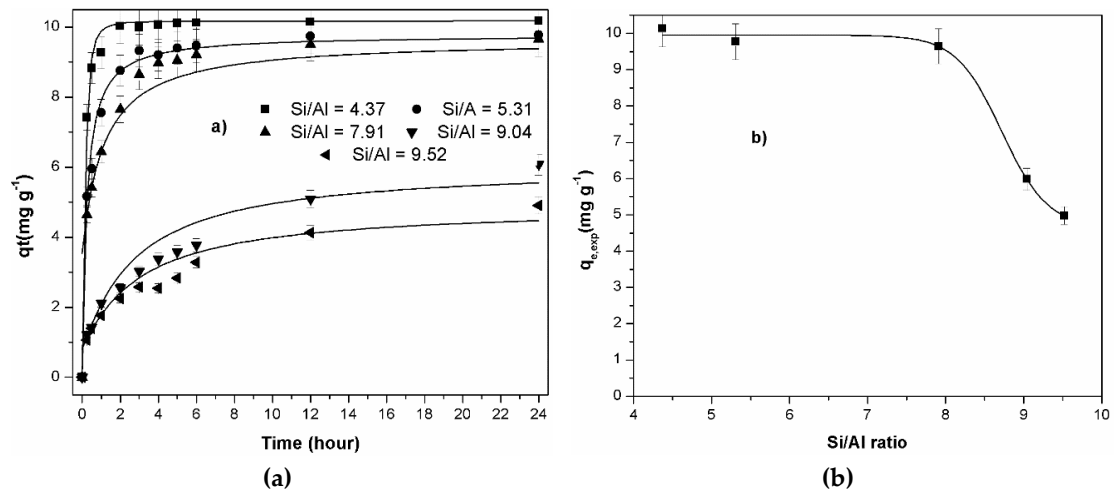


Figure 5. (a) Pb(II) uptake of vs. time and (b) experimental Pb(II) uptake vs. Si/Al ratio.

The results presented in Figure 5b show are similar in maximum Pb(II) uptake when the Si/Al ratio ranges from 4.3 to 7.91 shows. However, the sorption of Pb(II) decreased drastically as Si/Al ratio increased. This can be attributed to the decrease in exchangeable ions during the acid-treatment (Table 1) and higher competition between H^+ from the acid-modified clinoptilolite-rich-tuffs and Pb(II) in the solutions.

The data for Pb(II) sorption by non- and acid-modified clinoptilolite-rich tuffs were fitted to pseudo-first order, pseudo-second order, and intra-particle diffusion models. As shown in Table 2, the kinetic parameters corresponding to the sorption of Pb(II) by Nat-CLI, HCLI-0.1M, and HCLI-0.2 M fit best to the pseudo-second order model ($R^2 \geq 0.99$ and $q_{cal} \approx q_{exp}$), while for the HCLI-0.5 M and HCLI-1.0 M sorbents, the results show that the pseudo-first order model was more suitable for describing the kinetic process.

Table 2. Kinetic parameters for Pb(II) sorption by non- and acid-modified clinoptilolite-rich tuffs obtained by applying the pseudo-second order and pseudo-first order models.

Sample	Si/Al	Kinetic Models						
		Pseudo-Second Order				Pseudo-First Order		
		$q_e(\text{exp})$	$q_e(\text{cal})$	$k_2 \times 10^2$	R^2	$q_e(\text{cal})$	$k_1 \times 10^2$	R^2
Nat-CLI	4.37	10.14	10.21	2.39	1.0	0.53	0.27	0.60
HCLI-0.1 M	5.31	9.77	9.90	0.63	1.0	1.76	0.24	0.69
HCLI-0.2 M	7.91	9.64	9.82	0.40	0.99	2.53	0.23	0.76
HCLI-0.5 M	9.04	5.98	6.37	0.08	0.96	5.00	0.17	0.99
HCLI-1.0 M	9.52	4.98	5.25	0.11	0.97	3.97	0.21	0.99

Note: (exp) experimental data, (cal) calculated data; $q_e(\text{exp})$ and $q_e(\text{cal})$ in mg g^{-1} ; k_2 in $\text{g mg}^{-1}\text{min}^{-1}$; k_1 in min^{-1} .

The k_2 diminished when the Si/Al ratio increased. However, the k_1 slightly increased when the Si/Al increased as well. These results shows that the dealumination of the acid-modified clinoptilolite-rich tuff has repercussion on the kinetic of the Pb(II) sorption and the Si/Al ratio will determine the order of the kinetic reaction (pseudo-second order or pseudo-first order).

3.4. Isotherm

Figure 6 shows Pb(II) sorption by non- and acid-modified clinoptilolite-rich tuffs. It can be observed that the isotherms for the HCLI-0.1 M and HCLI-0.2 M were similar to those for Nat-CLI; whereas the isotherms for the Pb(II) sorption for HCLI-0.5 M and HCLI-1.0 M presented a different behavior. These differences can be attributed to the dealumination of the clinoptilolite-rich tuff after the treatment with 0.5 and 1.0 M H_2SO_4 solutions. The amount of aluminum in HCLI-0.5 M and HCLI-1.0 M were 1.7 and 2 times lower than Nat-CLI, respectively. In these cases, it is probably that the Ca^{2+} and K^+ from the zeolitic materials had played a role on the Pb(II) sorption.

The experimental equilibrium data for Pb(II) sorption by non- and acid-modified clinoptilolite-rich tuffs were fitted to the Langmuir and Freundlich models (Equations (4) and (5)) with the purpose of describing the sorption mechanism [6]. The values of the isotherm constants, including the determination coefficients (R^2), are summarized in Table 3. It was found that the Langmuir model better described Pb(II) uptake by Nat-CLI, HCLI-0.1 M, and HCLI-0.2 M ($R^2 \geq 0.99$). Comparison of the Langmuir constants (q_m) between non- and acid-modified clinoptilolite-rich tuffs, shows that Pb(II) removal decreases as Si/Al ratio increases ($q_m = 48.54, 37.037, \text{ and } 14.992 \text{ mg g}^{-1}$ for Si/Al = 4.37, 5.30, and 7.91, respectively). This result can be explained by the decrease in exchangeable ions from the zeolite network with the increase in sulfuric acid concentration due to the dealuminization of the zeolitic material or the greater competition of Pb(II) with the H^+ from the ion exchange sites in the zeolite network.

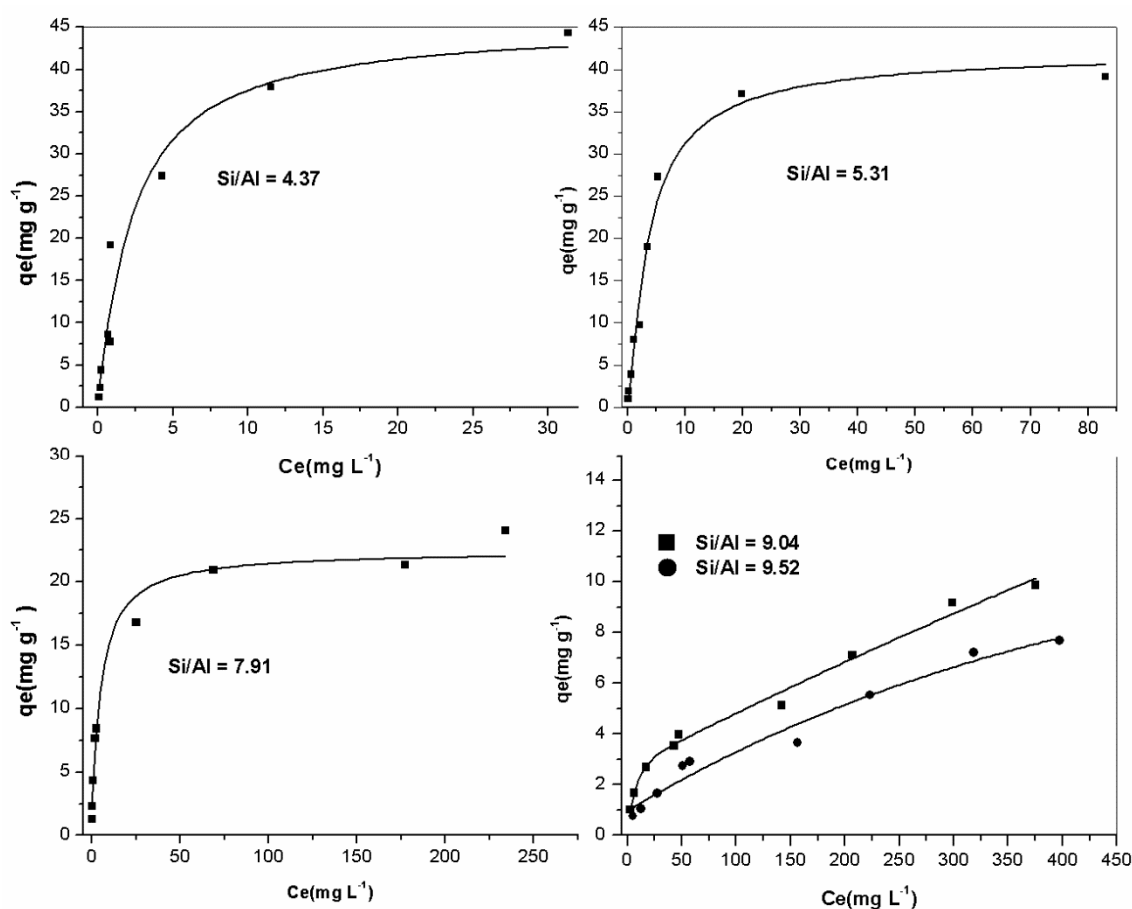


Figure 6. Isotherms for Pb(II) sorption of by non- and acid-modified clinoptilolite-rich tuffs.

Table 3. Description of Pb(II) sorption by Nat-CLI and H-CLI from the parameters obtained applying the Langmuir and Freundlich models.

Sample	Si/Al	Langmuir Isotherm		
		q_m (mg/g)	K_L (dm ³ /mg)	R^2
Nat-CLI	4.37	48.07	0.3598	0.9939
HCLI-0.1 M	5.31	41.49	0.2175	0.9970
HCLI-0.2 M	7.91	23.47	0.1969	0.9948
	9.04	10.67	0.0146	0.9163
	9.50	9.30	0.0081	0.8816
Freundlich Isotherm				
Sample	Si/Al	K_F (mg g ⁻¹) (L mg ⁻¹) ^{1/n}	n	R^2
HCLI-0.5 M	9.04	0.701	2.279	0.99
HCLI-1.0 M	9.52	0.295	1.849	0.98

For sorbents with Si/Al ratios of 9.05 and 9.52, the Freundlich isotherm adjusted better to the Pb(II) uptake ($0.99 \geq R^2 \geq 0.98$) than the Langmuir isotherm. This suggests that sorption did not occur on a uniform site; instead a multilayer sorption occurred in this system. Moreover, n values were between 1 and 10, indicating that the physical sorption of Pb(II) ions by acid-modified clinoptilolite-rich tuffs with Si/Al ratios of 9.04 and 9.5 is favorable [14]. It is important to mention that a unique mechanism is not involved on the sorption processes. For instance, the speciation of the heavy metal in solution, the surface charge of the sorbent as well as the nature and structure of the zeolitic materials could be some of the factors which are involved on the ion exchange or adsorption mechanisms.

Table 4 shows the maximum sorption capacity (q_m) of different materials for Pb(II) obtained from the Langmuir model at different initial concentrations, as was obtained in the present work. It can be observed that carbon foam has 10 times more sorption capacity than clinoptilolite-rich tuff for this heavy metal. However, the zeolitic material has 1.9 times more capacity to remove Pb(II) than pectin-containing substances. In the case of the acid-modified clinoptilolite-rich tuff the maximum sorption capacity is 5.1 times lower than that of the unmodified material. Other carbonaceous materials among them biochar, multi-walled carbon nanotubes functionalized by selenophosphoryl groups, and sultone-modified magnetic activated carbon, present similar maximum sorption capacities for Pb(II).

Table 4. Maximum sorption capacity of Pb(II) by materials with different nature.

Material	q_m (mg g ⁻¹)	Reference
Carbon foam	491.36	[42]
Biochar	151.5	[43]
Multi-walled carbon nanotubes functionalized by selenophosphoryl groups	149.25	[44]
Sultone-modified magnetic activated carbon	147.5	[45]
Pectin-containing substances	25.15	[46]
Clinoptilolite-rich tuff (Nat-CLI)	48.07	Present work
Clinoptilolite-rich tuff acidified using a solution 1.0 M of H ₂ SO ₄	9.30	Present work

3.5. Partition Coefficients

It was found that the partition coefficients have an inverse behavior with respect the Pb(II) initial concentration in aqueous solution, this means that the PC is high when the initial concentration is lower (Figure 7), because there are less Pb(II) in the solution to be sorbed in the preferential sites of the zeolitic networks before the saturation. It is important to mention that the determination coefficient (R^2) was 0.1468.

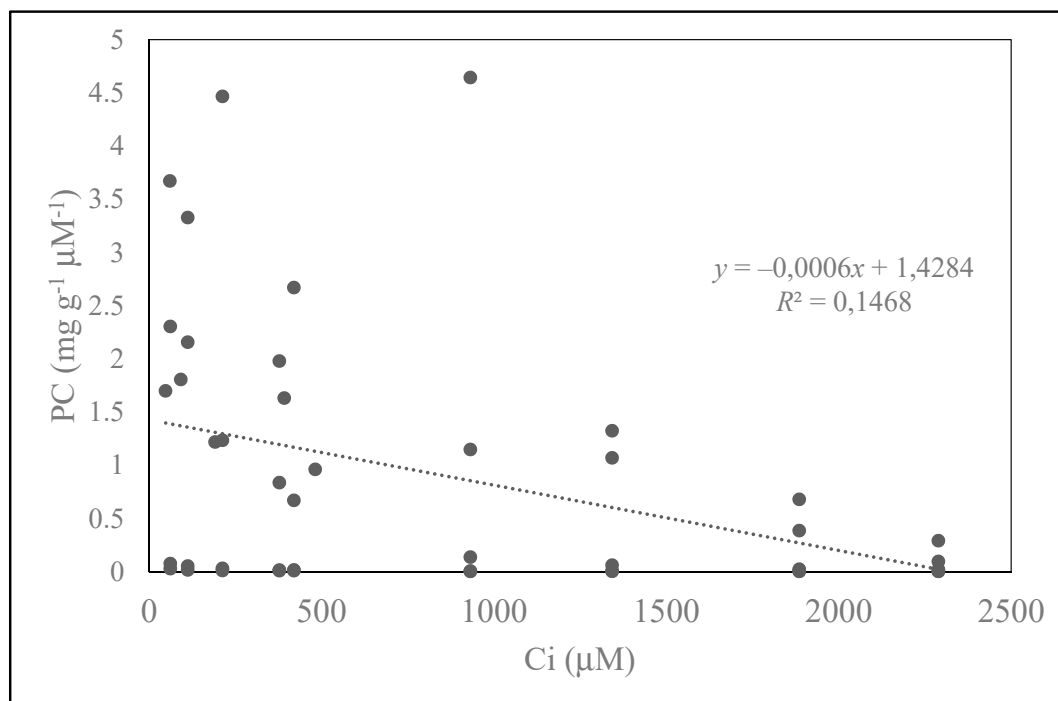


Figure 7. Partition coefficients for Pb(II) sorption by Nat-CLI and acid-modified clinoptilolite rich tuffs (PC) as a function of the initial concentration of lead in solution (Ci).

In Figure 8 it is observed that the Si/Al ratios of the clinoptilolite-rich tuffs notably affect the partition coefficients as a function of the initial concentration of the chemical specie of the heavy metal

in solution. For this reason, it is important to consider the ion exchange sites and the adsorption sites in each zeolite network before and after the treatment with 1.0 M of H_2SO_4 solutions for the removal of different chemical species from polluted water.

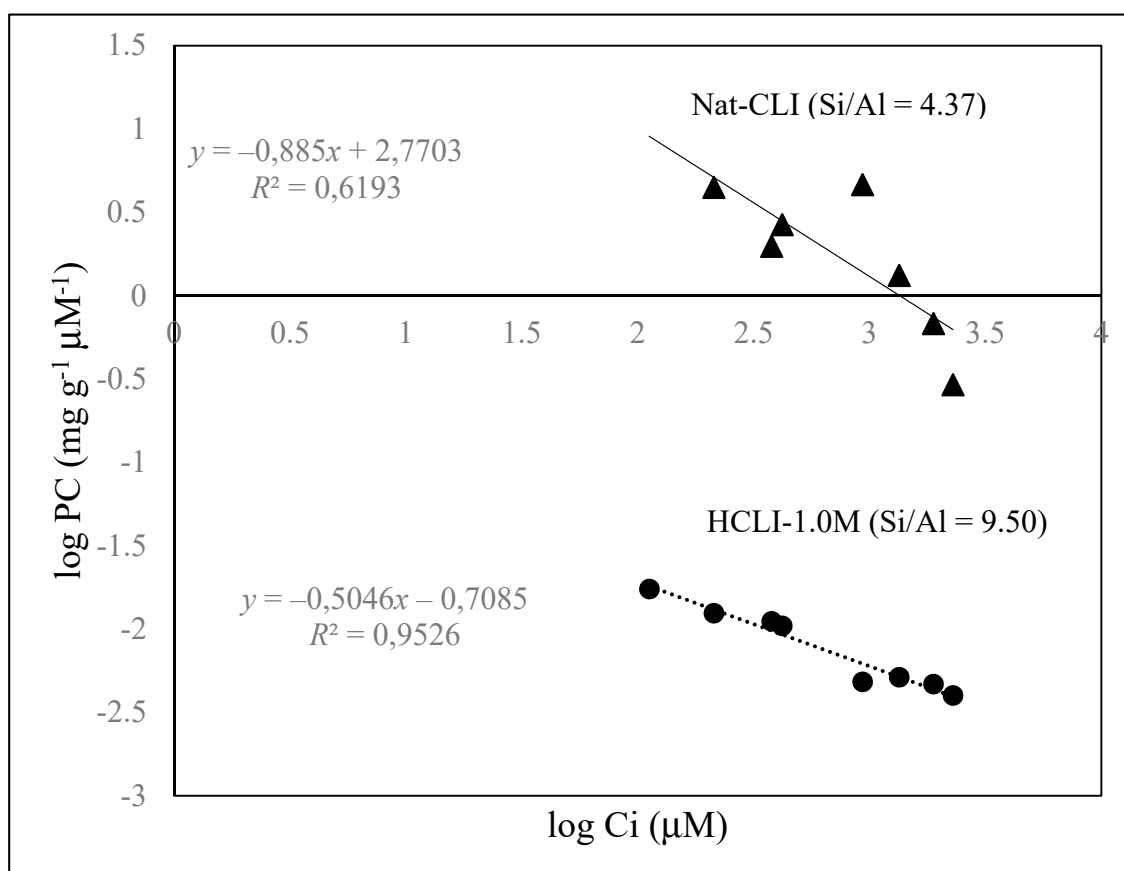


Figure 8. Comparison between the log PC for Nat-CLI and HCLI-1.0M as a function of log C_i of Pb(II) in solution.

3.6. Influence of Adsorbent Dosage

The percentage of Pb(II) uptake with respect to the non- and acid-modified clinoptilolite-rich tuffs dosages ($mg\ L^{-1}$) is shown in Figure 9. It can be observed that the dosage of all of the sorbents used is a very important parameter for Pb(II) uptake. The increment in sorption capacity was attributed to a higher number of available sorption sites [12]. In the case of sorbents with Si/Al ratios of 4.37, 5.31, and 7.91, sorption efficiency was highly dependent on increase in the sorbents dosage of solution up to $6\ mg\ L^{-1}$ when the maximum Pb(II) uptake percentage (99.99%) was achieved. For sorbents with a Si/Al ratio of 9.05 and 9.52, Pb(II) removal increases gradually with dosage, reaching 92.36% and 35.99%, respectively. One explanation of this behavior is the few available sorption sites in the zeolite networks of HCLI-0.5 M and HCLI-1.0 M to be occupied by the Pb(II) chemical species. The H-CLI1.0 M has the lowest amount of Al in the zeolitic material diminishing the ion exchange capacity. The amount of Ca^{2+} in the zeolitic material also drastically diminished, limiting the ion exchange: $Pb^{2+}_{(s)} + Ca^{2+}_{(z)} \rightarrow Pb^{2+}_{(z)} + Ca^{2+}_{(s)}$, where s represents the solution and z the zeolitic material. The sites where the K^+ are located into the zeolite network [47] do not favor the ion exchange with Pb^{2+} . Another explanation of this behavior is by the change of the nature of the zeolitic material from hydrophilic to hydrophobic character [36].

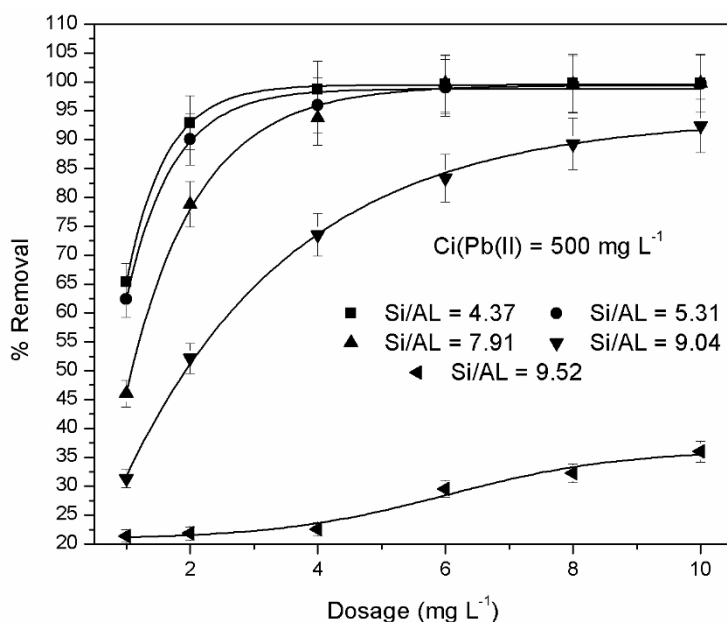


Figure 9. Effect of dosage of non- and acid-modified clinoptilolite-rich tuff on Pb(II) removal efficiency.

3.7. Effect of the Solution pH

The effect of initial solution pH on Pb(II) sorption by non- and acid-modified clinoptilolite-rich tuffs is illustrated in Figure 10. It can be observed that the curves presented in Figure 10a, all show a similar shape. For the first group, the removal percentage of Pb(II) increased by only 1.08%, 8.60%, and 9.47% in the pH range of 2–6, when the Si/Al ratio was 4.37, 5.31, and 7.91, respectively, while the maximum Pb(II) uptake percentage reached 97.92% to 99.58% for these sorbents at a solution pH of about 5. The lower removal capacity of Pb(II) at pH = 2 is due to a lower selectivity of clinoptilolite at a low pH and the strong competition between the Pb²⁺ and the H⁺ for the exchangeable sites on the clinoptilolite framework. The decrease in Pb(II) sorption at higher pH values can be explained by the formation of hydrolyzed Pb(II) species (K_{ps} of Pb(OH)₂ = 1.43×10^{-20}) which could precipitate or by the electrostatic repulsion between a possible negative Pb(II) species (Pb(OH)₃⁻ or Pb(OH)₄²⁻) and the negatively charged surface of the HCLI-0.5 M and HCLI-1.0 M zeolitic materials [48].

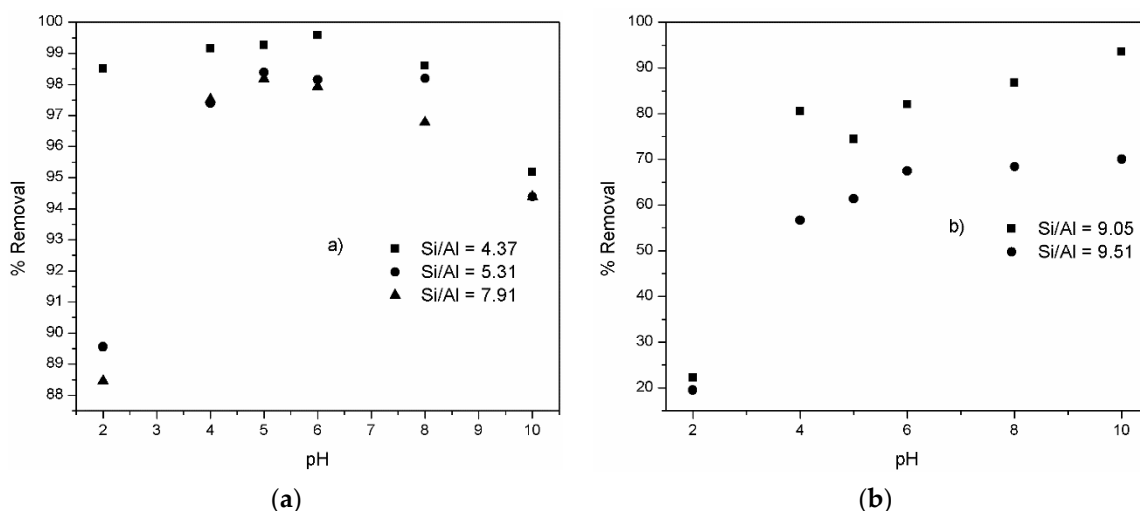


Figure 10. Effect of solution pH on Pb(II) sorption by samples with (a) Si/Al = 4.37, 5.31, and 7.91 and (b) Si/Al = 9.05 and 9.51.

For the second group (Figure 10b), which corresponds to sorbents with a Si/Al ratio of 9.05 and 9.52, solution pH has a significant influence on the Pb(II) uptake percentage. In the pH range of 2–6, the removal percentage of Pb(II) increases progressively from 22.22% to 82.02% and from 19.48% to 67.48% for Si/Al ratio of 9.05 and 9.53, respectively. At higher pH values, Pb(II) sorption increased continuously up to 93% and 70% for HCLI-0.5 M and HCLI-1.0 M, respectively. This can be attributed to the high acidity of these materials which has a beneficial effect, disfavoring the hydrolysis of the metal ions in the solution [12].

4. Conclusions

Nat-CLI, HCLI-0.1 M, HCL-0.2 M, HCLI-0.5 M, and HCLI-1.0 M are mainly composed of clinoptilolite; however, their crystallinity decreases with acid treatment.

FT-IR spectra also are in good agreement with the about reduction of crystallinity of HCL due to the dealumination of Nat-CLI that take place after its acid treatment.

The ions from natural zeolite (Na^+ , K^+ , Ca^{2+} , and Mg^{2+}) decrease significantly with increasing H_2SO_4 concentration to obtain acid-modified natural zeolite which promoted an increase in Si/Al ratios.

The pH_{PZC} value is affected by acid treatment, which decrease for all the acid-modified clinoptilolite-rich tuffs in comparison with Nat-CLI.

Sorption of Pb(II) is achieved after a short contact time (200 min) for the samples with a Si/Al ratio between 4.31 to 7.91; whereas the equilibrium time for the samples with Si/Al ratios from 9.05 to 9.51 is approximately 700 min. The Pb(II) sorption kinetic for Nat-CLI, HCLI-0.1 M, and HCL-0.2 M well fits to the pseudo-second order model, while for HCLI-0.5 M and HCLI-1.0 M the Pb(II) sorption is better described applying the pseudo-first order model.

Isotherm suggests that the Pb(II) sorption process for Nat-CLI, HCLI-0.1 M, and HCL-0.2 M are well described by the Langmuir model. The maximum sorption capacity of samples with Si/Al ratios of 4.37, 5.31, and 7.91 are 48.54, 37.04, and 14.99 mg g^{-1} , respectively. The experimental data fit better to the Freundlich model for the sorbents with Si/Al ratio of 9.05 and 9.53.

The Nat-CLI, HCLI-0.1M and HCL-0.2M with a dosage of 6 g L^{-1} show an excellent and similar ability to remove Pb(II). Sorption efficiency is also dependent on the dosage of HCLI-0.5 M and HCLI-1.0 M. At 10 mg L^{-1} , the maximum sorption capacity reaches approximately 92.36% and 36%, respectively.

Maximum removal of Pb(II) by Nat-CLI, HCLI-0.1 M, and HCL-0.2 M occur in a range of 6–8; whereas for HCLI-0.5 M and HCLI-1.0 M the Pb(II) uptake also takes place at higher pH values.

Acid modified clinoptilolite with Si/Al ratio values of 9.05 and 9.51 may be used as a low-cost and abundant resource for Pb(II) removal from basic wastewaters such as those produced by the textile industry and may provide an alternative to more costly materials.

Author Contributions: M.A. and M.T.O. conceived and planned the experiments; M.A. wrote the manuscript with input from all authors. M.T.O. contributed to the analysis and interpretation of the results. A.V.C.Q., A.R.V.-O., J.V., F.A.-F. and G.G.-V. carried out the characterization of the samples and the interpretation of the results. All authors provided critical feedback and helped shape the research, analysis and manuscript.

Funding: This research was funded by National Council of Science and Technology of Mexico grant numbers 169133 and 254665.

Conflicts of Interest: The authors declare no conflict of interest.

References

1. Krajisnik, D.; Milojević-Rakić, M.; Malenović, A.; Daković, A.; Ibric, S.; Savić, S.; Dondur, V.; Matijašević, S.; Radulović, A.; Daniels, R.; et al. Cationic surfactants-modified natural zeolites: Improvement of the excipients functionality. *Drug Dev. Ind. Pharm.* **2010**, *36*, 1215–1224. [[CrossRef](#)] [[PubMed](#)]
2. Mansoor, E.; Van Der Mynsbrugge, J.; Head-Gordon, M.; Bell, A.T. Impact of long-range electrostatic and dispersive interactions on theoretical predictions of adsorption and catalysis in zeolites. *Catal. Today* **2018**, *312*, 51–65. [[CrossRef](#)]

3. Wang, S.; Peng, Y. Natural zeolites as effective adsorbents in water and wastewater treatment. *Chem. Eng. J.* **2010**, *156*, 11–24. [[CrossRef](#)]
4. Louis, B.; Walspurger, S.; Sommer, J. Quantitative Determination of Brønsted Acid Sites on Zeolites: A New Approach Towards the Chemical Composition of Zeolites. *Catal. Lett.* **2004**, *93*, 81–84. [[CrossRef](#)]
5. Zhong, J.; Han, J.; Wei, Y.; Tian, P.; Guo, X.; Song, C.; Liu, Z. Recent advances of the nano-hierarchical SAPO-34 in the methanol-to-Olefin (MTO) reaction and other applications. *Catal. Sci. Technol.* **2017**, *7*, 4905–4923. [[CrossRef](#)]
6. Sprynskyy, M.; Buszewski, B.; Terzyk, A.P.; Namie, J. Study of the selection mechanism of heavy metal (Pb^{2+} , Cu^{2+} , Ni^{2+} , and Cd^{2+}) adsorption on clinoptilolite. *J. Colloid Interface Sci.* **2006**, *304*, 21–28. [[CrossRef](#)]
7. Jiang, N.; Shang, R.; Heijman, S.G.; Rietveld, L.C. High-silica zeolites for adsorption of organic micro-pollutants in water treatment: A review. *Water Res.* **2018**, *144*, 145–161. [[CrossRef](#)] [[PubMed](#)]
8. Garrido-Ramírez, E.; Theng, B.; Mora, M. Clays and oxide minerals as catalysts and nanocatalysts in Fenton-like reactions—A review. *Appl. Clay Sci.* **2010**, *47*, 182–192. [[CrossRef](#)]
9. Reháková, M.; Čuvanová, S.; Dzivák, M.; Rimár, J.; Gaval'ová, Z. Agricultural and agrochemical uses of natural zeolite of the clinoptilolite type. *Curr. Opin. Solid State Mater. Sci.* **2004**, *8*, 397–404. [[CrossRef](#)]
10. Erdem, E.; Karapinar, N.; Donat, R. The removal of heavy metal cations by natural zeolites. *J. Colloid Interface Sci.* **2004**, *280*, 309–314. [[CrossRef](#)]
11. Vocciante, M.; D'Auris, A.D.F.; Finocchi, A.; Tagliabue, M.; Bellettato, M.; Ferrucci, A.; Reverberi, A.P.; Ferro, S.; D'Auris, A.D.F. Adsorption of ammonium on clinoptilolite in presence of competing cations: Investigation on groundwater remediation. *J. Clean. Prod.* **2018**, *198*, 480–487. [[CrossRef](#)]
12. Abatal, M.; Olguin, M.T.; Abdellaoui, Y.; Bouari, A.E. Sorption of Cd(II), Ni(II) and Zn(II) on natural, sodium-, and acid-Modified clinoptilolite-Rich tuff. *Env. Prot. Eng.* **2018**, *44*, 41–59.
13. Abatal, M.; Olguin, M.T. Evaluating of effectiveness of a natural and modified surface mexican clinoptilolite-rich tuff in removing phenol and p-Nitrophenol from aqueous solutions. *Environ. Prot. Eng.* **2012**, *38*, 53–65.
14. Abatal, M.; Olguin, M.T. Comparison of lead removal from aqueous solution between natural-, sodium-, and acid-modified clinoptilolite-rich tuffs. *Desalin. Water Treat.* **2017**, *72*, 318–327. [[CrossRef](#)]
15. Doula, M.; Ioannou, A. The effect of electrolyte anion on Cu adsorption-desorption by clinoptilolite. *Microporous Mesoporous Mater.* **2003**, *58*, 115–130. [[CrossRef](#)]
16. Ates, A.; Akgül, G. Modification of natural zeolite with NaOH for removal of manganese in drinking water. *Powder Technol.* **2016**, *287*, 285–291. [[CrossRef](#)]
17. Dakovi, A.; Gatta, G.D.; Rotiroti, N. Applied Surface Science Characterization of lead sorption by the natural and Fe (III)-modified zeolite. *Appl. Surf. Sci.* **2013**, *283*, 764–774.
18. Garcia-Basabe, Y.; Rodriguez-Iznaga, I.; De Menorval, L.-C.; Llewellyn, P.; Maurin, G.; Lewis, D.W.; Binions, R.; Autie, M.; Ruiz-Salvador, A.R. Step-wise dealumination of natural clinoptilolite: Structural and physicochemical characterization. *Microporous Mesoporous Mater.* **2010**, *135*, 187–196. [[CrossRef](#)]
19. Matsui, M.; Kiyozumi, Y.; Mizushina, Y.; Sakaguchi, K.; Mizukami, F. Adsorption and desorption behavior of basic proteins on zeolites. *Sep. Purif. Technol.* **2015**, *149*, 103–109. [[CrossRef](#)]
20. Tsai, W.-T.; Hsu, H.-C.; Su, T.-Y.; Lin, K.-Y.; Lin, C.-M. Adsorption characteristics of bisphenol-A in aqueous solutions onto hydrophobic zeolite. *J. Colloid Interface Sci.* **2006**, *299*, 513–519. [[CrossRef](#)]
21. Zhao, X.S.; Ma, Q.; Lu, G.Q. (Max) VOC Removal: Comparison of MCM-41 with Hydrophobic Zeolites and Activated Carbon. *Energy Fuels* **1998**, *12*, 1051–1054. [[CrossRef](#)]
22. Abelló, S.; Bonilla, A.; Pérez-Ramírez, J. Mesoporous ZSM-5 zeolite catalysts prepared by desilication with organic hydroxides and comparison with NaOH leaching. *Appl. Catal. A Gen.* **2009**, *364*, 191–198. [[CrossRef](#)]
23. Ateş, A. Effect of alkali-treatment on the characteristics of natural zeolites with different compositions. *J. Colloid Interface Sci.* **2018**, *523*, 266–281. [[CrossRef](#)] [[PubMed](#)]
24. Malekian, R.; Abedi-Koupai, J.; Eslamian, S.S.; Mousavi, S.F.; Abbaspour, K.C.; Afyuni, M. Ion-exchange process for ammonium removal and release using natural Iranian zeolite. *Appl. Clay Sci.* **2011**, *51*, 323–329. [[CrossRef](#)]
25. Gili, M.B.Z.; Conato, M.T. Adsorption uptake of mordenite-type zeolites with varying Si/Al ratio on Zn^{2+} ions in aqueous solution. *Mater. Res. Express* **2019**, *6*, 045508. [[CrossRef](#)]

26. Ong, L.H.; Dömök, M.; Olindo, R.; van Veen, A.C.; Lercher, J.A. Microporous and Mesoporous Materials Dealumination of HZSM-5 via steam-Treatment. *Microporous Mesoporous Mater.* **2012**, *164*, 9–20. [[CrossRef](#)]
27. Müller, J.M.; Mesquita, G.C.; Franco, S.M.; Borges, L.D.; de Macedo, J.L.; Dias, J.A.; Dias, S.C.L. Microporous and Mesoporous Materials Solid-State dealumination of zeolites for use as catalysts in alcohol dehydration. *Microporous Mesoporous Mater.* **2015**, *204*, 50–57. [[CrossRef](#)]
28. Kuwahara, Y.; Aoyama, J.; Miyakubo, K.; Eguchi, T.; Kamegawa, T.; Mori, K.; Yamashita, H. TiO₂ photocatalyst for degradation of organic compounds in water and air supported on highly hydrophobic FAU zeolite: Structural, sorptive, and photocatalytic studies. *J. Catal.* **2012**, *285*, 223–234. [[CrossRef](#)]
29. Wang, C.; Cao, L.; Huang, J. Influences of acid and heat treatments on the structure and water vapor adsorption property of natural zeolite. *Surf. Interface Anal.* **2017**, *49*, 1249–1255. [[CrossRef](#)]
30. Matias, P.; Couto, C.S.; Graça, I.; Lopes, J.M.; Carvalho, A.P.; Ribeiro, F.R.; Guisnet, M. Applied Catalysis A: General Desilication of a TON zeolite with NaOH: Influence on porosity, acidity and catalytic properties. *Appl. Catal. A Gen.* **2011**, *399*, 100–109. [[CrossRef](#)]
31. Kussainova, M.Z.; Chernyakov, R.M.; Jussipbekov, Z.U.; Pas, S. Structural investigation of raw clinoptilolite over the Pb²⁺ adsorption process from phosphoric acid. *J. Mol. Struct.* **2019**, *1184*, 49–58. [[CrossRef](#)]
32. Ma, W.; Ya, F.-Q.; Han, M.; Wang, R. Characteristics of equilibrium, kinetics studies for adsorption of fluoride on magnetic-chitosan particle. *J. Hazard. Mater.* **2007**, *143*, 296–302. [[CrossRef](#)] [[PubMed](#)]
33. Ho, Y.-S.; Chiu, W.-T.; Wang, C.-C. Regression analysis for the sorption isotherms of basic dyes on sugarcane dust. *Bioresour. Technol.* **2005**, *96*, 1285–1291. [[CrossRef](#)] [[PubMed](#)]
34. Treacy, M.M.J.; Higgins, J.B. *Collection of Simulated Xrd Powder Patterns For Zeolites*, 4th ed.; Elsevier: Amsterdam, The Netherlands, 2001.
35. Cobzaru, C.; Oprea, S.; Dumitriu, E.; Hulea, V. Gas phase aldol condensation of lower aldehydes over clinoptilolite rich natural zeolites. *Appl. Catal. A Gen.* **2008**, *351*, 253–258. [[CrossRef](#)]
36. Wang, C.; Leng, S.; Guo, H.; Cao, L.; Huang, J. Applied Surface Science Acid and alkali treatments for regulation of hydrophilicity/hydrophobicity of natural zeolite. *Appl. Surf. Sci.* **2019**, *478*, 319–326. [[CrossRef](#)]
37. Peng, S.; Hao, K.; Han, F.; Tang, Z.; Niu, B.; Zhang, X.; Wang, Z.; Hong, S. Enhanced removal of bisphenol-AF onto chitosan-modified zeolite by sodium cholate in aqueous solutions. *Carbohydr. Polym.* **2015**, *130*, 364–371. [[CrossRef](#)] [[PubMed](#)]
38. Elaiopoulos, K.; Perraki, T.; Grigoropoulou, E. Microporous and Mesoporous Materials Monitoring the effect of hydrothermal treatments on the structure of a natural zeolite through a combined XRD, FTIR, XRF, SEM and N₂-Porosimetry analysis. *Microporous Mesoporous Mater.* **2010**, *134*, 29–43. [[CrossRef](#)]
39. Rožić, M.; Cerjan-Stefanović, Š.; Kurajica, S.; Mačefat, M.R.; Margeta, K.; Farkaš, A. Decationization and dealumination of clinoptilolite tuff and ammonium exchange on acid-Modified tuff. *J. Colloid Interface Sci.* **2005**, *284*, 48–56. [[CrossRef](#)]
40. Pechar, F.; Rykl, D. Infrared spectra of natural zeolites of the stilbite group. *Chem. Pap.* **1981**, *35*, 189–202.
41. Stojanović, M.; Matijašević, S.; Zildžović, S.; Stojanović, J.; Došić, M.; Nikolić, J.; Stojanović, M.; Labus, N. Removal of uranium (VI) from aqueous solution by acid modified zeolites. *Zastita Materijala* **2016**, *57*, 551–558.
42. Lee, C.-G.; Jeon, J.-W.; Hwang, M.-J.; Ahn, K.-H.; Park, C.; Choi, J.-W.; Lee, S.-H. Lead and copper removal from aqueous solutions using carbon foam derived from phenol resin. *Chemosphere* **2015**, *130*, 59–65. [[CrossRef](#)] [[PubMed](#)]
43. Wongrod, S.; Simon, S.; Guibaud, G.; Lens, P.N.; Pechaud, Y.; Huguenot, D.; Van Hullebusch, E.D. Lead sorption by biochar produced from digestates: Consequences of chemical modification and washing. *J. Environ. Manag.* **2018**, *219*, 277–284. [[CrossRef](#)] [[PubMed](#)]
44. Kończyk, J.; Źarska, S.; Ciesielski, W. Adsorptive removal of Pb(II) ions from aqueous solutions by multi-walled carbon nanotubes functionalised by selenophosphoryl groups: Kinetic, mechanism, and thermodynamic studies. *Colloids Surf. A: Physicochem. Eng. Asp.* **2019**, *575*, 271–282. [[CrossRef](#)]
45. Nejadshafiee, V.; Islami, M.R. Adsorption capacity of heavy metal ions using sultone-modified magnetic activated carbon as a bio-adsorbent. *Mater. Sci. Eng. C* **2019**, *101*, 42–52. [[CrossRef](#)] [[PubMed](#)]
46. Koksharov, S.A.; Aleeva, S.V.; Lepilova, O.V. Description of adsorption interactions of lead ions with functional groups of pectin-containing substances. *J. Mol. Liq.* **2019**, *283*, 606–616. [[CrossRef](#)]

47. Wang, X.; Plackowski, C.A.; Nguyen, A.V. X-ray photoelectron spectroscopic investigation into the surface effects of sulphuric acid treated natural zeolite. *Powder Technol.* **2016**, *295*, 27–34. [[CrossRef](#)]
48. Yang, X.; Yang, S.; Yang, S.; Hu, J.; Tan, X.; Wang, X. Effect of pH, ionic strength and temperature on sorption of Pb(II) on NKF-6 zeolite studied by batch technique. *Chem. Eng. J.* **2011**, *168*, 86–93. [[CrossRef](#)]



© 2019 by the authors. Licensee MDPI, Basel, Switzerland. This article is an open access article distributed under the terms and conditions of the Creative Commons Attribution (CC BY) license (<http://creativecommons.org/licenses/by/4.0/>).